Quantum metrology via partial quantum error correction

Yinan Chen,[1,*] Zongyuan Wang,[2,†] and Sisi Zhou[3,4,‡]

[1] *Department of Physics and Institute for Quantum Information and Matter, California Institute of Technology, Pasadena, California, 91125, USA*

[2] *International Center for Quantum Materials, School of Physics, Peking University, Beijing 100871, China*

[3] *Perimeter Institute for Theoretical Physics, Waterloo, Ontario, N2L 2Y5, Canada*

[4] *Department of Physics and Astronomy, Department of Applied Mathematics, and Institute for Quantum Computing, University of Waterloo, Ontario N2L 3G1, Canada*

(Dated: June 10, 2026)

We introduce a method for error-corrected quantum metrology where only *partial* quantum error correction (QEC) is needed to suppress local noise and maintain the probe states' super-standard-quantum-limit (super-SQL) sensing performance. This stands in contrast to the existing QEC-assisted sensing schemes in *Phys. Rev. Lett. 112, 080801 (2014)* and *Phys. Rev. Lett. 112, 150802 (2014)*, where a probe state is encoded into the logical subspace of a quantum code and error correction involves measurements on all checks of the code. Here, we encode the probe states into superpositions of energetically different states of the underlying quantum code. For our probe states, error correction using a subset of checks is enough to suppress noise both before and after phase imprinting. We analyze the tradeoff in noise suppression. For noise parallel to our phase imprinter of weight l, we achieve a suppression of p^δ where p is the noise strength and $\delta = \lfloor (l+1)/2 \rfloor$. We propose an adaptive imprinter weight increasing strategy to maintain super-SQL performance as we scale up the system. In all our examples, checks and phase imprinters are chosen to be local operators avoiding non-local connectivity.

arXiv:2605.08341v2 [quant-ph] 10 Jun 2026

Introduction— Quantum metrology is one of the central components of quantum technology. It exploits many-body entanglement to estimate one or more parameters of a quantum system beyond the classically achievable limit, the standard quantum limit (SQL) [1–4]. The fundamental precision for such estimation tasks is given by the quantum Fisher information (QFI) [5]. For a probe state ρ_θ imprinted with an unknown parameter θ, the estimation error is lower bound by the Cramér–Rao bound (CRB) [6] $\delta\theta \geq 1/\sqrt{F_q[\rho_\theta]}$ where $F_q[\rho_\theta]$ is the QFI of ρ_θ. A larger QFI leads to a higher achievable precision. Without entanglement, QFI scales at best linearly with the size of the probe system N (i.e. $F_q[\rho_\theta] \sim N$), which yields the SQL bound of $\delta\theta \geq 1/\sqrt{N}$. On the other hand, if the probe state is an entangled many-body state, then the ultimate quantum mechanically achievable limit, the Heisenberg Limit (HL), of $\delta\theta \geq 1/N$ is obtainable, i.e. $F_q[\rho_\theta] \sim N^2$. We will call the scaling of $F_q[\rho_\theta] \sim N^\nu$ for $1 < \nu \leq 2$ super-SQL [7].

However, good probe states, such as the Greenberger–Horne–Zeilinger (GHZ) state [8], are susceptible to noise [9–14]. They can easily decohere, and thus, lose their ability to perform high precision estimations. Error-corrected quantum metrology addresses exactly this problem. Using techniques of quantum error-correction, we may preserve the entangled structure of the probe states before and after phase imprinting. Until now, the main methodology of error-corrected quantum metrology is to encode the GHZ state into the logical subspace of M quantum codes as $|\mathrm{GHZ}\rangle_L = \frac{1}{\sqrt{2}}\left(|0\rangle_L^{\otimes M} + |1\rangle_L^{\otimes M}\right)$ for $M \in \mathbb{Z}_{\geq 1}$ [15–17]. To maintain the logical GHZ state, one requires error-correction using all checks of the code(s).

Here, through examples, we argue that full quantum error correction as in Refs. [15–17] is not necessary for metrology. A *partial* quantum error correction on the underlying quantum codes is enough to suppress the noise and to maintain the super-SQL precision. Specifically, we encode the GHZ state into a probe state that is a superposition of two energetically different states of the quantum code. We show that a judicious selection of checks together with one additional operator called the *optimal measurement* or *symmetry operator* [18], commuting with the selected checks, is enough to perform error-correction on such a probe state and to maintain super-SQL precision. Moving beyond the full error correction protocols [15–17], we can suppress both perpendicular and parallel noise to our imprinter before and after phase imprinting. After phase imprinting, error correction for the parallel noise is impossible [19]. However, we can suppress the parallel noise at the cost of both increased operator weight for the phase imprinter and reduced sensing performance against the perpendicular noise. We present our examples in terms of quantum codes familiar in quantum computation, providing a proposal for an application of quantum computation platforms for metrological purposes [20–24].

This Letter is organized as follows. We begin by presenting our GHZ-like probe states in the context of Calderbank–Shor–Steane (CSS) codes [25, 26]. We discuss how perpendicular and parallel noises can be suppressed while preserving super-SQL sensitivity. Then, we present our partial error correction protocols together with our adaptive weight strategy to maintain super-SQL as the system scales. We first discuss noise at the stage

of after perfect state preparation but prior to phase imprinting. We assume perfect measurements. We focus on the 2D toric codes and the Bacon-Shor codes, although our scheme generalizes straightforwardly to other quantum codes supporting our construction. We finish with a discussion of noise after phase imprinting.

The probe state— Every stabilizer generator of a CSS code can be arranged into either a product of Pauli-X operators or a product of Pauli-Z operators as $\langle S_{X,i}, S_{Z,j}\rangle$ where i, j index the stabilizer generators. We construct a GHZ-like probe state as [27]

$$|\mathrm{CSS}\rangle = \frac{1}{\sqrt{2}}\Big(|S_Z = 1\cdots 1\rangle + |S_Z = -1\cdots -1\rangle \Big), \quad (1)$$

where $|S_Z = 1\cdots 1\rangle$ is the $+1$ eigenstate of all $S_{X,i}$'s and all the $S_{Z,j}$'s, and $|S_Z = -1\cdots -1\rangle$ is the eigenstate with $+1$ for all $S_{X,i}$'s but -1 for all $S_{Z,j}$'s. We denote the number of S_X as N_X and that of S_Z as N_Z. To simplify the presentation of our scheme, we assume that all S_Z have the same weight l for the rest of this Letter. We also assume there is an X-type operator T_X having odd overlap with every chosen Z-type check. T_X is therefore a symmetry of $|\mathrm{CSS}\rangle$ i.e. $T_X|\mathrm{CSS}\rangle = |\mathrm{CSS}\rangle$. The imprinter is chosen as $U(\theta) = \exp\left[i\theta \sum_j S_{Z,j}\right]$, which is a product of local unitaries $\exp[i\theta S_{Z,i}]$ whose support is the i-th Z-type check. The QFI for the pure state $|\mathrm{CSS}\rangle$ with respect to $U(\theta)$ is $F_q = 4N_Z^2$, saturating the Cramér–Rao bound. The corresponding SQL, $4N_Z$, is defined as the QFI of the product state $[\frac{1}{\sqrt{2}}(|S_Z = 1\rangle + |S_Z = -1\rangle)]^{\otimes N_Z}$. Later in this work, we also use HL and SQL with respect to the number of *physical* qubits by replacing $N_Z \to N$ where N stands for the number of physical qubits. We note that although T_X is a global operator, there exists a method to measure it, through an ancilla system, by local operators [28], see also Remark 3 in the Supplemental Material (SM).

For the above $|\mathrm{CSS}\rangle$, the optimal measurement can be chosen as T_X [11]. Note that since we have used all the S_Z stabilizers for the imprinter, we can no longer use them for error correction. Specifically, we use S_X for error correction either before or after phase imprinting, since $[S_X, S_Z] = 0$. The T_X measurement is performed only before phase imprinting to prepare the probe state in Eq. (1). After phase imprinting, it is instead used as the optimal measurement for phase readout. Its optimality is discussed in the SM.

Perpendicular and parallel noise in partial error correction— We discuss the i.i.d. perpendicular (X) and i.i.d. parallel (Z) errors acting on $|\mathrm{CSS}\rangle$, prior to phase imprinting. We denote local dephasing along Z the parallel error because it commutes with the imprinter $U(\theta)$. We begin by discussing error occurring before phase imprinting as this represents the most destructive effect [29, 30]. We monitor only the S_X syndromes and correct only the i.i.d. dephasing noise $E_{Z,j}[\rho] = (1-p)\rho + pZ_j\rho Z_j$ where p is the noise strength. As the syndrome measurement and recovery channel commute with the imprinter $U(\theta)$, error correction can be conducted in any stage during sensing before the final measurement using T_X. Here, we apply error correction right before the final measurement and discuss the effect on sensing under i.i.d. X/Z noise.

i.i.d. *X*-noise. Although partial error correction acts trivially here, we begin with the general observation: For errors before phase imprinting, HL scaling is always maintained if the noise channel respects T_X, namely $T_X \prod_i E_i(\rho) = \prod_i E_i(\rho) T_X = \prod_i E_i(\rho)$ with $\rho = |\mathrm{CSS}\rangle\langle\mathrm{CSS}|$ [11, 31]. For the i.i.d. X noise, the variance of $O_S = \sum_j S_{Z,j}$ is evaluated via the dual-channel: $\mathrm{Tr}[\prod_i E_{X,i}(\rho) O_S^2] = \mathrm{Tr}[\rho \prod_i E_{X,i}^\dagger(O_S^2)] = \sum_{j,k} \mathrm{Tr}[\rho \prod_i E_{X,i}^\dagger(S_{Z,j}S_{Z,k})]$, where $E_i^\dagger$ denotes the dual channel of E_i. If the local error E_i commutes with $S_{Z,j}S_{Z,k}$, it acts trivially and $E_{X,i}^\dagger(S_{Z,j}S_{Z,k}) = S_{Z,j}S_{Z,k}$; otherwise, it yields $(1-2p)S_{Z,j}S_{Z,k}$. QFI under i.i.d. X noise then takes the form $F_{q,X} = \alpha N_Z^2 + \mathcal{O}(N_Z)$ with $\alpha = 4(1-2p)^{2l}$, where l is the weight of S_Z stabilizer generators [11] (see also SM). Importantly, the prefactor α is an $\mathcal{O}(1)$ function of the stabilizer weight l and p, which does not scale with N_Z, confirming that HL (w.r.t. N_Z) is reachable. We note that the conclusion applies to other noise channels as long as the symmetry is strongly preserved. Finally, the i.i.d. X noise after phase imprinting $U(\theta)$ does not change QFI, since $E_{X,j}^\dagger[T_X] = T_X$ and the CRB remains intact.

i.i.d. *Z*-noise. For errors that do not preserve the T_X symmetry, residual error patterns with $T_X = -1$ lead to dephasing. For i.i.d. Z noise, error correction based on the X syndromes leaves residual patterns equivalent either to products of Z stabilizers or to logical Z operators. We focus on the regime where dephasing is dominated by small contractible loops, and hence logical Z errors are neglected. A residual loop containing an odd number of Z stabilizers produces a π-phase jump, $\langle T_X\rangle_{\mathrm{CSS}} \to -\langle T_X\rangle_{\mathrm{CSS}}$.

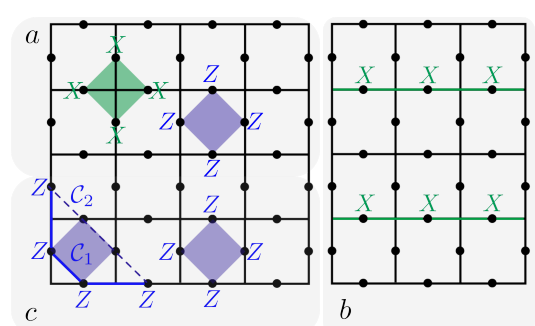

FIG. 1. An example of the toric-code protocol. (a) vertex S_X stabilizers, plaquette S_Z stabilizers. (b) construction of the detection operator $\prod_{j\in -} X_j$. (c) a false choice of the path $\mathcal{C}_2$ (dashed line) forms a dephasing loop of Z errors with the string $\mathcal{C}_1$ (solid line).

For $p \ll 1$, the leading local stabilizer-sector dephasing probability can be estimated by considering two types of events. First, an error pattern may form a full Z stabilizer $S_{Z,i}$ of weight l, with probability proportional to p^l. Second, and typically dominantly, an error pattern may occupy at least half of the qubits in some $S_{Z,i}$, causing the decoder to choose an incorrect matching path and thereby induce a local dephasing event; see Fig. 1. This contribution scales as $p^{\lfloor (l+1)/2 \rfloor}$. Thus, neglecting logical errors and higher-order correlations, we approximate the error-plus-correction process by an effective i.i.d. S_Z-dephasing channel with $p_{\text{eff}} = cp^\delta + O(p^{\delta+1})$, where $\delta = \lfloor (l+1)/2 \rfloor$ and $c = \mathcal{O}(1)$ depends on the geometry and decoder. The QFI under this i.i.d.-S_Z channel scales as: $F_{q,Z} = 4(1-2cp^\delta)^{2N_Z} N_Z^2$. In general, for large lattice size N_Z, $F_{q,Z}$ decays exponentially. Nevertheless, the polynomial suppression of the effective noise strength, $p \to p^\delta$, is already an improvement resulting from error correction. See the SM for a detailed analysis of $F_{q,Z}$ and the decoding schemes.

***X/Z* trade-off.** We find the following trade-off: For fixed l, we have seen the HL scaling, with respect to the number of stabilizers, of the QFI $F_{q,X}$ under i.i.d. X noise, which persists up to $p = 0.5$ where it drops to the SQL $4N_Z$ (w.r.t. the number of stabilizers). On the other hand, the QFI under i.i.d. Z noise is much closer to the HL at small p due to the extra suppression p^δ in $F_{q,Z}$. The leading order for $F_{q,Z}$ and $F_{q,X}$ at the noise strength p_s is determined by $(1-2p_s)^{2l}$ and $(1-cp_s^\delta)^{2N_Z}$. Increasing l then suppresses the $F_{q,X}$ while boosting $F_{q,Z}$ exponentially closer to 1. We therefore ask: *is there an optimal choice of l for different numbers of physical qubits such that both $F_{q,X}$ and $F_{q,Z}$ perform better than the SQL?* In comparison with the full QEC [15–17], we remark that although perpendicular noises are usually viewed benign [32], it becomes highly relevant when increasing the weight of the phase imprinter. In the next subsection, we treat the X and Z noise on equal footing and show that partial error correction can answer the above question in the affirmative.

The protocols — We now discuss examples of the partial QEC scheme. We begin with the trivial example of bare GHZ protocol where error correction is trivial and then move on to the toric code and Bacon-Shor code.

GHZ state. As a warm-up, we start with the case where $|0\rangle_L = |0\rangle^{\otimes N}$, $S_{Z,i} = Z_i$, and $T_X = \prod_j X_j$. The projection onto the $+1$ eigenspace of T_X yields the GHZ state $|\text{GHZ}\rangle = \frac{1}{\sqrt{2}}\left[|0\rangle^{\otimes N} + |1\rangle^{\otimes N}\right]$. We treat this as the trivial CSS code with no S_X at all. The phase imprinter is the standard $U(\theta) = e^{i\theta \sum_j Z_j}$. Under the i.i.d. X channel $\mathcal{E}_X = \prod_j \mathcal{E}_{X,j}$ that respects the symmetry operator $T_X = \prod_j X_j$, the QFI equals four times the variance of $\sum_j Z_j$ of the output state. Using the dual channel trick, we obtain $\prod_j \mathcal{E}^*_{x,j}\left[\left(\sum_i Z_i\right)^2\right] = (1-2p)^2\left(\sum_i Z_i\right)^2 + \mathcal{O}(N)$, which gives the QFI $F_{q,X} = 4(1-2p)^2N^2 + 16p(1-p)N$ at $l = 1$. The computation of $F_{q,X}$ follows the steps in [11] and is given in the SM. The i.i.d. Z noise is the most detrimental as $\delta = 1$ gives no noise suppression, leading to $F_{q,Z} = 4(1-2p)^{2N}N^2$.

Toric code. The Hamiltonian of the toric code is [33, 34] $H = -\sum_v S_{X,v} - \sum_p S_{Z,p}$, where $S_{X,v} = \prod_{j\in v} X_j$ and $S_{Z,p} = \prod_{j\in p} Z_j$ are the vertex and plaquette stabilizers respectively. The phase imprinter is chosen as the sum of all plaquette stabilizers $O_S = \sum_p S_{Z,p}$. Due to the $e-m$ duality, choosing $O_S = \sum_v S_{X,v}$ would yield identical results under interchanging i.i.d. X and Z noises. The optimal measurement can be chosen as any X patterns that share an odd overlap with each S_Z stabilizer. In Fig. 1b, we illustrate one such operator, which is defined as $T_X = \prod_{j\in -} X_j$. In Fig. 1c, we show an example of incorrectly assigning a correction path that leads to a dephasing loop of S_Z.

On the square lattice, each S_Z stabilizer has weight four, giving $F_{q,X} = 4(1-2p)^8N_Z^2 + 4\left[1+4(1-2p)^6 - 5(1-2p)^8\right]N_Z$. For Z noise, partial error correction suppresses the leading local stabilizer-sector dephasing rate to $p_{\text{eff}} \sim \alpha p^\delta$, with $\delta = \lfloor (4+1)/2 \rfloor = 2$, so that, at small p and neglecting logical error events, $F_{q,Z} \simeq 4(1-\alpha p^2)^{2N_Z}N_Z^2$; see Fig. 2a and the SM.

In Fig. 2b, we plot $F_{q,Z}/F_{q,X}$ for systems with $2N_Z = 12$ to $2N_Z = 36$ physical qubits, together with the physical-qubit SQL normalized by $F_{q,X}$. The saturation of SQL/$F_{q,X} \to 2$ reflects that the number of physical qubits is twice the number of S_Z stabilizers. The X/Z

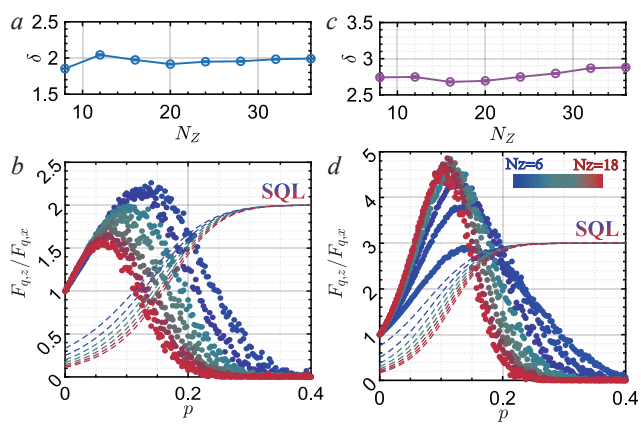

FIG. 2. QFI for toric codes on the square and the honeycomb lattices under different Pauli noise. (a) fitted exponent δ in $F_q = 4(1-cp^\delta)^{2N_Z}N_Z^2$ for toric codes on square lattices. (b) $F_{q,Z}/F_{q,X}$ ratio as a function of p for toric codes with $2N_Z = 12$ to $2N_Z = 36$ physical qubits on square lattices. The dashed curve is the ratio between the SQL and $F_{q,X}$. (c) fitted exponent δ for toric codes on hexagonal lattices. (d) $F_{q,Z}/F_{q,X}$ as a function of p for toric codes with $3N_Z = 18$ to $3N_Z = 54$ physical qubits on hexagonal lattices. For simulation, we used periodic boundary conditions and the Minimum-Weight-Perfect Matching (MWPM) decoder for decoding (see SM). The density matrix is obtained from 10^4 error patterns.

trade-off is clear: increasing N_Z enhances $F_{q,X}$ but suppresses $F_{q,Z}$, although $F_{q,Z}$ remains well above the uncorrected GHZ benchmark in the regime considered.

For the $F_{q,Z}$ numerics, we prepare $|\mathrm{CSS}\rangle$, apply i.i.d. Z noise, measure the $S_{X,v}$ syndromes, perform partial error correction, and compute the QFI with respect to $\sum_p S_{Z,p}$. Error patterns yielding logical Z_L errors are discarded, because these logical error events are sufficiently suppressed (see SM).

A natural question to ask is whether δ can be increased further by increasing l. To address this, we consider the toric code on a honeycomb lattice, where each S_Z stabilizer is weight-6 (while each S_X is weight-3). Choosing the phase imprinter as $O_S = \sum_p S_{Z,p}$, the QFI under i.i.d. X noise is $F_{q,X} = 4(1-2p)^{12}N_Z^2 + 4\left[1+6(1-2p)^{10}-7(1-2p)^{12}\right]N_Z$, while under i.i.d. Z noise we model it via $F_{q,Z} = 4(1-cp^3)^{2N_Z}N_Z^2$ (Fig. 2c). In Fig. 2d, we plot the ratio $F_{q,Z}/F_{q,X}$ between them for systems with $3N_Z = 18$ to $3N_Z = 54$ physical qubits, where the SQL approaches $3F_{q,X}$, reflecting the use of $3N_Z$ physical qubits.

Fig. 2c shows the suppression δ as a function of $3N_Z$: Since each $S_{Z,p}$ stabilizer contains 6 qubits, effective dephasing occurs only when at least 3 qubits dephase, leading to $\delta \to 3$ and enhancing $F_{q,Z}$ compared with the same code on square-lattices.

Improvement comes with costs. By the X/Z tradeoff, increasing l unavoidably suppresses $F_{q,X}$. As shown in Fig. 2b and d, the QFI under i.i.d. X noise drops below the SQL once the dashed curves exceed unity. Thus, although $F_{q,Z}$ remains above the SQL for larger N_Z and p when increasing l from 4 to 6, $F_{q,X}$ falls below the SQL for smaller system size and smaller noise strength. Consequently, one cannot increase the stabilizer weight l indefinitely if we want to keep both $F_{q,Z}$ and $F_{q,X}$ above the SQL. In the next example, we show that the value of l to optimize $F_{q,Z}$ indeed leads to a sub-SQL $F_{q,X}$. Nevertheless, we can employ an adaptive strategy to increase l while maintaining both QFIs above the SQL.

Bacon-Shor code. Consider the Bacon–Shor CSS subsystem code [35, 36] on an $m \times n$ periodic lattice, with local two-qubit gauge generators $g^X_{i,j} = X_{i,j}X_{i+1,j}$ and $g^Z_{i,j} = Z_{i,j}Z_{i,j+1}$. The corresponding X-type stabilizers are $S^X_i = \prod_{j=1}^n X_{i,j}X_{i+1,j}$. Although these X-type stabilizers are not normally measured in the Bacon–Shor code for quantum computation, here they are instead selected as the phase-imprinting terms $O_S = \sum_i S^X_i$. We work in a highly anisotropic regime $m \gg n$, with n kept small or increased only slowly with m. Hence, each imprinter term S^X_i is supported on a local $2 \times n$ strip of weight $2n$, rather than on a system-spanning operator. Partial error correction is then performed by measuring the local Z-type gauge checks $g^Z_{i,j}$, while the optimal measurement is chosen as the Z-type operator $T_Z = \prod_i Z_{2i-1,1}$. Since the phase imprinter is now built from X-type stabilizers, the roles of X and Z are exchanged relative to the previous examples. This yields $F_{q,Z} = 4(1-2p)^{4n}m^2 + 4\left[1+2(1-2p)^{2n}-3(1-2p)^{4n}\right]m$ and $F_{q,X} = 4\left[1-2\sum_{k=0}^{\lfloor\frac{n-1}{2}\rfloor}\binom{n}{k}p^k(1-p)^{n-k}\right]^{2m} m^2$ [37]. Note that since O_S is chosen as the sum of all S_X stabilizers, the i.i.d. X noise is now *parallel* and the i.i.d. Z noise *perpendicular*.

The X/Z trade-off is evident. To suppress the parallel noise, n has to be increased, which reduces the QFI under the perpendicular noise. The simplest way to see this is by taking $n \to \infty$, we recover $F_{q,Z} = 4m$ that is exactly the SQL and $F_{q,X} = 4m^2$ that is exactly the HL. Nevertheless, we note they are defined with respect to m, which is the number of S_X stabilizers. In the Bacon-Shor code, this number is much less than the number of $g^Z_{i,j}$ checks or that of the physical qubits.

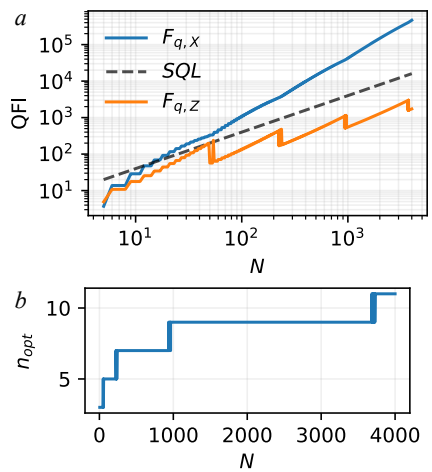

FIG. 3. X/Z trade-off. (a) optimal quantum Fisher information $F_{q,X}$ under i.i.d. X noise and the corresponding $F_{q,Z}$ under i.i.d. Z noise. Here, the X noise is the parallel one. (b) optimal stabilizer weight $n_{opt} = l_{opt}/2$ as a function of physical qubits at $p = 0.08$.

In Fig. 3a, we plot the maximal QFI as a function of the number of physical qubits, $N = nm$, under i.i.d. X noise ($F_{q,X}$) and its counterpart under i.i.d. Z noise ($F_{q,Z}$). Although increasing N helps to preserve the enhanced scaling of $F_{q,X}$, the perpendicular noise ultimately dominates, leading to scaling that drops below the SQL. In Fig. 3b, we plot the optimal stabilizer weight n_{opt} as a function of N, which follows the logarithmic behavior predicted in Ref. [15]. This X/Z trade-off implies that the stabilizer weight should not be increased indefinitely under partial error correction.

We can, however, apply an adaptive and balanced growth of the stabilizer weight such that both $F_{q,X}$ and $F_{q,Z}$ remain above the SQL. For example, Fig. 4 shows this procedure for increasing values of the noise strength p. Starting from $n = 3$, we keep the stabilizer weight unchanged unless $F_{q,X}$ drops to the SQL. After this, we increase n by 2 which yields jumps in QFI. Although such

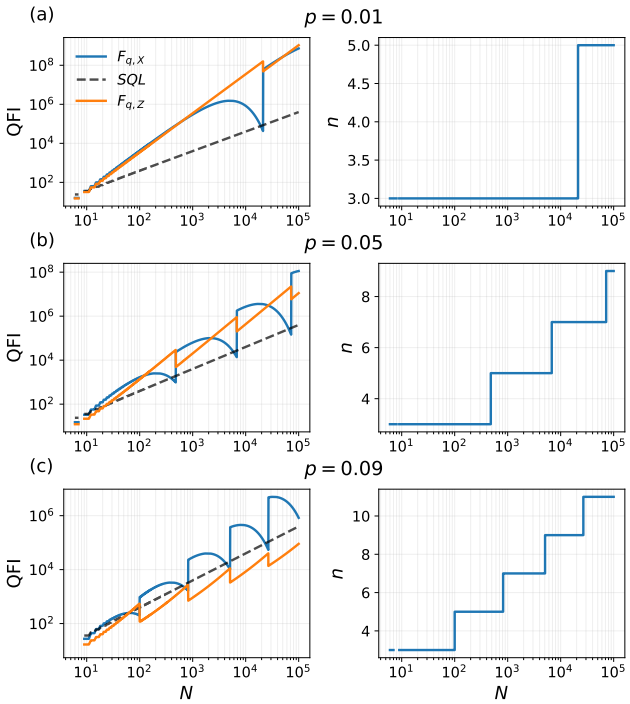

FIG. 4. Optimization of the QFI (left panels) for the Bacon-Shor code (m, n) via an adaptive stabilizer-weight increasing scheme, (a)–(c). The parameter $n = l/2$ (right panels) is adaptively increased by 2 once $F_{q,X}$ hits SQL. For small p, this adaptive strategy keeps both $F_{q,X}$ and $F_{q,Z}$ above SQL. For $p > 0.09$, scaling advantage in $F_{q,Z}$ is lost.

a slow increase in n reduces $F_{q,X}$ compared to the optimal in Fig. 3, it enables super-SQL scalings in both $F_{q,X}$ and $F_{q,Z}$ (provided that $p < 0.09$ where $F_{q,Z}$ drops below the SQL similar to Fig. 3), making the Bacon-Shor code robust to both the parallel and the perpendicular noise. We emphasize that this scaling advantage is not limited to small pN, but persists even for $N = 10^7$ with $pN \gg 1$.

More generally, as explained in the SM, the QFI under a mixture of i.i.d. X and i.i.d. Z noise is the multiplicative average of $F_{q,X}$ and $F_{q,Z}$ as $F_{q,XZ} = F_{q,X}F_{q,Z}/4N_Z^2$. We thus expect QEC to keep the QFI subject to the mixed X, Z noise above the SQL for $\nu^X + \nu^Z > 3$ where $F_{q,X} \sim N^{\nu^X}$ and $F_{q,Z} \sim N^{\nu^Z}$ with $\nu^X, \nu^Z > 1$. When this asymptotic condition is not satisfied, a super-SQL QFI can still be maintained provided the noise strength remains below the finite-noise threshold analyzed in the SM.

This adaptive strategy also applies to the toric code protocol. Increasing l corresponds to arranging qubits into different lattices. Here we present the cases of $l = 4$ and $l = 6$, and this construction can be extended to larger l, e.g. the square-octagonal lattice with $l = 8$ [38]. Alternatively, one may consider other CSS codes, such as 2D color codes [21, 39, 40], which gives $l = 6$ while requiring fewer physical qubits, leading to a more efficient protocol.

Noise after phase imprinting— We now discuss noise occurring after phase imprinting. In this case, we instead need to protect the evolved probe state $|\mathrm{CSS}\rangle \to |\mathrm{CSS}_\theta\rangle = \frac{1}{\sqrt{2}}\left[e^{iN_Z\theta}|S_Z = 1\cdots 1\rangle + e^{-iN_Z\theta}|S_Z = -1\cdots -1\rangle\right]$, which leaves the $+1$ eigenspace of T_X in general. However, since the stabilizers commute, we can also perform error correction using only the S_X stabilizers without washing out the phase information. In this case, the QFI becomes significantly more robust against perpendicular noise, based on the following observation: The QFI $F_q = 4N_Z^2$ is intact under an error channel $\prod_j E_j$ if its dual channel has trivial action on the detection operator T_X i.e. $\prod_j E_j^\dagger(T_X) = T_X$. The proof is straightforward by noting that $\mathrm{Tr}\left[\prod_j E_j(\rho_\theta)T_X\right] = \mathrm{Tr}\left[\rho_\theta \prod_j E_j^\dagger(T_X)\right] = \mathrm{Tr}\left[\rho_\theta T_X\right]$. Identifying $\rho_\theta = |\mathrm{CSS}_\theta\rangle\langle\mathrm{CSS}_\theta|$, we restore $\mathrm{Tr}\left[\prod_j E_j(\rho_\theta)T_X\right] = \cos(2N_Z\theta)$. For parallel noise, the situation is the same as before because the phase imprinter commutes with the error channel. Moreover, we can lower bound the QFI for arbitrary i.i.d. Pauli errors

Theorem 1. *The QFI of the probe state ρ_θ under i.i.d. Pauli errors described by $E_P[\rho_\theta] = (1 - p_x - p_y - p_z)\rho_\theta + p_x X\rho_\theta X + p_y Y\rho_\theta Y + p_z Z\rho_\theta Z$ + partial error correction is lower bounded by the QFI under the i.i.d. dephasing channel $\mathcal{E}_z[\rho_\theta] = (1-p)\rho_\theta + pZ\rho_\theta Z$ + partial error correction with the identification $p = p_y + p_z$.*

We prove this theorem in the SM. We then conclude that the perpendicular error after the phase imprinter is benign to the QFI, and the sensing performance can always be improved by increasing the stabilizer weight to suppress the parallel noise.

Conclusion— In this Letter, we introduced a new scheme for error-corrected quantum metrology built on the idea of *partial* quantum error correction. We analyzed the tradeoff of noise suppression. For parallel noise with strength p, we achieved p^δ suppression with $\delta > 1$. We proposed an adaptive strategy to maintain beyond classical performance as we scale up the system. Additional remarks are presented in the SM.

We thank Sara Murciano and Pablo Sala for insightful discussions. Z.W. is supported by the National Natural Science Foundation of China (Grant No. 12474491) and the Central University Fundamental Research Funds (Peking University). S.Z. acknowledges support from National Research Council of Canada (Grant No. AQC-217-1) and Perimeter Institute for Theoretical Physics, a research institute supported in part by the Government of Canada through the Department of Innovation, Science and Economic Development Canada and by the Province of Ontario through the Ministry of Colleges and Universities.

* Equal contribution; yinanc@caltech.edu
† Equal contribution; zongyuan.wang15@outlook.com
‡ sisi.zhou26@gmail.com

[1] W. Wasilewski, K. Jensen, H. Krauter, J. J. Renema, M. V. Balabas, and E. S. Polzik, "Quantum noise limited and entanglement-assisted magnetometry," Phys. Rev. Lett. **104**, 133601 (2010).
[2] Florian Wolfgramm, Alessandro Cerè, Federica A. Beduini, Ana Predojević, Marco Koschorreck, and Morgan W. Mitchell, "Squeezed-light optical magnetometry," Phys. Rev. Lett. **105**, 053601 (2010).
[3] J. Aasi *et al.*, "Enhanced sensitivity of the ligo gravitational wave detector by using squeezed states of light," Nat. Photonics **7**, 613–619 (2013).
[4] M. Tse *et al.*, "Quantum-enhanced advanced ligo detectors in the era of gravitational-wave astronomy," Phys. Rev. Lett. **123**, 231107 (2019).
[5] Géza Tóth, "Multipartite entanglement and high-precision metrology," Phys. Rev. A **85**, 022322 (2012).
[6] Philipp Hauke, Markus Heyl, Luca Tagliacozzo, and Peter Zoller, "Measuring multipartite entanglement through dynamic susceptibilities," Nature Physics **12**, 778–782 (2016).
[7] We note that in the presence of noise, the scaling behavior depends on the quantum codes, the noise strength, and the imprinter. We analyze this when we present our example protocols.
[8] Vittorio Giovannetti, Seth Lloyd, and Lorenzo Maccone, "Quantum metrology," Phys. Rev. Lett. **96**, 010401 (2006).
[9] Jian Ma, Yi-xiao Huang, Xiaoguang Wang, and C. P. Sun, "Quantum fisher information of the greenberger-horne-zeilinger state in decoherence channels," Phys. Rev. A **84**, 022302 (2011).
[10] Yinan Chen, Andreas Elben, Angel Rubio, and Gil Refael, "Bosonic entanglement and quantum sensing from energy transfer in two-tone floquet systems," Phys. Rev. Res. **7**, 043014 (2025).
[11] Yinan Chen, Sara Murciano, Pablo Sala, and Jason Alicea, "Quantum sensing with critical systems: impact of symmetry, imperfections, and decoherence," (2026), arXiv:2601.04364.
[12] Yang Wang and Barbara M. Terhal, "Preparing dicke states in a spin ensemble using phase estimation," Phys. Rev. A **104**, 032407 (2021).
[13] Andrea López-Incera, Pavel Sekatski, and Wolfgang Dür, "All macroscopic quantum states are fragile and hard to prepare," Quantum **3**, 118 (2019).
[14] Rafał Demkowicz-Dobrzański, Jan Kołodyński, and Mădălin Guţă, "The elusive Heisenberg limit in quantum-enhanced metrology," Nature Communications **3**, 1063 (2012).
[15] W. Dür, M. Skotiniotis, F. Fröwis, and B. Kraus, "Improved quantum metrology using quantum error correction," Phys. Rev. Lett. **112**, 080801 (2014).
[16] E. M. Kessler, I. Lovchinsky, A. O. Sushkov, and M. D. Lukin, "Quantum error correction for metrology," Phys. Rev. Lett. **112**, 150802 (2014).
[17] Roee Ozeri, "Heisenberg limited metrology using quantum error-correction codes," (2013), arXiv:1310.3432 [quant-ph].
[18] The terminology "optimal measurement" comes from Ref. [11]. It is the measurement operator, given the probes states and the imprinters, that saturates the CRB. In this Letter, the optimal measurement operator is the strong symmetry (see Ref. [41] for definition in condensed matter physics) operator of the probe state by construction. Hence, we use the two names interchangeably.
[19] Sisi Zhou, Mengzhen Zhang, John Preskill, and Liang Jiang, "Achieving the heisenberg limit in quantum metrology using quantum error correction," Nature Communications **9**, 78 (2018).
[20] Google Quantum AI and Collaborators, "Quantum error correction below the surface code threshold," Nature **638**, 920–926 (2025).
[21] N. Lacroix, A. Bourassa, F. J. H. Heras, L. M. Zhang, J. Bausch, A. W. Senior, T. Edlich, N. Shutty, *et al.*, "Scaling and logic in the colour code on a superconducting quantum processor," Nature **645**, 614–619 (2025).
[22] Dolev Bluvstein, Alexandra A. Geim, Sophie H. Li, Simon J. Evered, J. Pablo Bonilla Ataides, *et al.*, "A fault-tolerant neutral-atom architecture for universal quantum computation," Nature **649**, 39–46 (2026).
[23] Ben W. Reichardt, Adam Paetznick, David Aasen, Ivan Basov, Juan M. Bello-Rivas, Parsa Bonderson, Rui Chao, *et al.*, "Fault-tolerant quantum computation with a neutral atom processor," (2025), arXiv:2411.11822 [quant-ph].
[24] Anthony Ransford, M. S. Allman, Jake Arkinstall, J. P. Campora III, Samuel F. Cooper, Robert D. Delaney, Joan M. Dreiling, *et al.*, "Helios: A 98-qubit trapped-ion quantum computer," (2025), arXiv:2511.05465 [quant-ph].
[25] Andrew Steane, "Multiple-particle interference and quantum error correction," Proceedings of the Royal Society A: Mathematical, Physical and Engineering Sciences **452**, 2551–2577 (1996).
[26] A. R. Calderbank and Peter W. Shor, "Good quantum error-correcting codes exist," Phys. Rev. A **54**, 1098–1105 (1996).
[27] We note that the construction requires the two stabilizer sectors appearing in Eq. (1) to be nonempty. In particular, if the chosen Z-type checks obey relations of the form $\prod_j S_{Z,j} = I$, then the assigned eigenvalues s_j must satisfy $\prod_j s_j = 1$. Thus, the all--1 sector is allowed only when every such relation contains an even number of checks. More generally, when stabilizer constraints obstruct the all--1 sector, one may instead choose a nearby allowed syndrome sector, for example by flipping or omitting $O(1)$ selected checks, provided all stabilizer constraints remain satisfied. Such a finite modification changes the generator-eigenvalue separation only by $O(1)$, and therefore does not affect the leading N_Z-scaling.
[28] Dominic J. Williamson and Theodore J. Yoder, "Low-overhead fault-tolerant quantum computation by gauging logical operators," Nature Physics **22**, 598–603 (2026).
[29] Animesh Datta, Lijian Zhang, Nicholas Thomas-Peter, Uwe Dorner, Brian J. Smith, and Ian A. Walmsley, "Quantum metrology with imperfect states and detectors," Physical Review A **83** (2011), 10.1103/physreva.83.063836.
[30] Shane Dooley, William J. Munro, and Kae Nemoto, "Quantum metrology including state preparation

and readout times," Physical Review A **94** (2016), 10.1103/physreva.94.052320.

[31] Irénée Frérot and Tommaso Roscilde, "Symmetry: A fundamental resource for quantum coherence and metrology," Phys. Rev. Lett. **133**, 260402 (2024).

[32] Chao Zhang, Thomas R. Bromley, Yun-Feng Huang, Huan Cao, Wei-Min Lv, Bi-Heng Liu, Chuan-Feng Li, Guang-Can Guo, Marco Cianciaruso, and Gerardo Adesso, "Demonstrating quantum coherence and metrology that is resilient to transversal noise," Phys. Rev. Lett. **123**, 180504 (2019).

[33] A.Yu. Kitaev, "Fault-tolerant quantum computation by anyons," Annals of Physics **303**, 2–30 (2003).

[34] S. B. Bravyi and A. Yu. Kitaev, "Quantum codes on a lattice with boundary," (1998), arXiv:quant-ph/9811052 [quant-ph].

[35] Dave Bacon, "Operator quantum error-correcting subsystems for self-correcting quantum memories," Phys. Rev. A **73**, 012340 (2006).

[36] Panos Aliferis and Andrew W. Cross, "Subsystem fault tolerance with the bacon-shor code," Phys. Rev. Lett. **98**, 220502 (2007).

[37] This is a harsh estimate of the $F_{q,X}$ following the argument for repetition codes in [15], as the Bacon-Shor code doubles the weight of imprinter $2n$ and dephasing on any single row/column does not change the QFI. Nevertheless, we show that, even for this harsh estimation, it is possible to keep both $F_{q,X}$ and $F_{q,Z}$ above the SQL by arranging the shape (m, n).

[38] Zongyuan Wang, Xiuqi Ma, David T. Stephen, Michael Hermele, and Xie Chen, "Renormalization of ising cagenet model and generalized foliation," Phys. Rev. B **108**, 035148 (2023).

[39] H. Bombin and M. A. Martin-Delgado, "Topological quantum distillation," Phys. Rev. Lett. **97**, 180501 (2006).

[40] Markus S. Kesselring, Fernando Pastawski, Jens Eisert, and Benjamin J. Brown, "The boundaries and twist defects of the color code and their applications to topological quantum computation," Quantum **2**, 101 (2018).

[41] Leonardo A. Lessa, Ruochen Ma, Jian-Hao Zhang, Zhen Bi, Meng Cheng, and Chong Wang, "Strong-to-weak spontaneous symmetry breaking in mixed quantum states," PRX Quantum **6**, 010344 (2025).

[42] Roland Krischek, Christian Schwemmer, Witlef Wieczorek, Harald Weinfurter, Philipp Hyllus, Luca Pezzé, and Augusto Smerzi, "Useful multiparticle entanglement and sub-shot-noise sensitivity in experimental phase estimation," Phys. Rev. Lett. **107**, 080504 (2011).

[43] Iagoba Apellaniz, Bernd Lücke, Jan Peise, Carsten Klempt, and Géza Tóth, "Detecting metrologically useful entanglement in the vicinity of dicke states," New Journal of Physics **17**, 083027 (2015).

[44] Himanshu Sahu, Qian Xu, and Sisi Zhou, "Achieving the heisenberg limit using fault-tolerant quantum error correction," (2026), arXiv:2601.05457 [quant-ph].

[45] R. Chaves, J. B. Brask, M. Markiewicz, J. Kołodyński, and A. Acín, "Noisy metrology beyond the standard quantum limit," Phys. Rev. Lett. **111**, 120401 (2013).

[46] Sammy Ragy, Marcin Jarzyna, and Rafał Demkowicz-Dobrzański, "Compatibility in multiparameter quantum metrology," Phys. Rev. A **94**, 052108 (2016).

[47] Rafał Demkowicz-Dobrzański, Wojciech Górecki, and Mădălin Guţă, "Multi-parameter estimation beyond quantum fisher information," Journal of Physics A: Mathematical and Theoretical **53**, 363001 (2020).

Supplemental Materials

REMARKS

Remark 1. In this work, we introduced a sensing method that utilizes only partial QEC on the probe states constructed from CSS codes to achieve enough noise suppression to retain the probe states' super-SQL sensing performance. The main results are summarized as follows.

- **Analytical expression for QFI, $F_{q,X}$, under perpendicular noise.**
  Building on the symmetry argument in Ref. [11], we analytically computed the QFI under perpendicular noise that (strongly) preserves the symmetry of the probe state, with an explicit and exact dependence on the stabilizer weight l. Although $F_{q,X}$ always exhibits super-SQL scaling with respect to the number of stabilizers, it falls below the SQL when expressed in terms of the number of physical qubits for sufficiently large l. This means that we cannot increase l indefinitely to suppress parallel noise.

- **Improvement for QFI, $F_{q,Z}$, under parallel noise.**
  In contrast to the perpendicular case, increasing the stabilizer weight l always enhances $F_{q,Z}$, since dephasing becomes uncorrectable only when at least half of the qubits in a stabilizer are affected. This leads to a polynomial suppression of the noise strength, $p \to \alpha p^{\delta}$, with $\delta > 1$. This suppression arises from QEC and is demonstrated numerically for three CSS codes: the toric code on square and honeycomb lattices and the (m, n) Bacon–Shor code. Following Ref. [15], we recover super-SQL scaling with respect to the number of physical qubits, provided that the stabilizer weight increases logarithmically, $l \sim \log N$. However, such an increase in l may lead to sub-SQL scaling in $F_{q,X}$, reflecting a trade-off between robustness to parallel and perpendicular noise.

- **An adaptive method to maintain super-SQL performance under both noise types.**
  Building on the (m, n) Bacon–Shor code, we numerically showed that a more refined scaling of $l(N)$ can balance the performance of $F_{q,X}$ and $F_{q,Z}$. In particular, increasing the stabilizer weight by 2 only when the parallel-noise QFI hits the SQL allows both $F_{q,X}$ and $F_{q,Z}$ to remain above the SQL for small noise strength $p < 0.09$. This threshold is independent of N, and the enhanced scaling persists up to $N = 10^7$, where $pN \gg 1$. Furthermore, we prove rigorously that the QFI under a general mixture of X and Z noise is the multiplicative average of $F_{q,X}$ and $F_{q,Z}$: $F_{q,XZ} = \frac{F_{q,X} F_{q,Z}}{4N_Z^2}$, which implies partial error correction is able to preserve the QFI above the SQL under a mixture of perpendicular and parallel noise.

- **Noise suppression after phase imprinting**
  We also considered the case where errors occur after phase imprinting, and showed that increasing the stabilizer weight l suppresses general i.i.d. Pauli errors. Although we focused on probe states constructed from CSS codes, our approach applies more broadly to other metrologically useful states. For example, one could encode the Dicke states [42, 43]. Furthermore, since a gradual increase in l—even slower than logarithmic growth in N—is sufficient for robustness (see Fig. 4 in the Letter), the phase imprinter can be viewed as a sum of *local* operators, making it potentially feasible on platforms that support both QEC and local parameter encoding, such as superconducting-qubit architectures [20, 21] and neutral atom platforms [22, 23]. This suggests that local codes developed for quantum computation can also be advantageous in metrological settings.

Remark 2. We note that not all partial QEC protocols beat the bare GHZ protocol. For example, consider the Bacon-Shor code whose Hamiltonian is given in the main text. If we choose the phase imprinter to be $O_S = \sum_{i,j} g^Z_{i,j}$, the optimal measurement to be $T_X = \prod_{i,j} X_{i,2j-1}$, and choose the $S_{X,i}$ stabilizers for performing error correction, then this choice of operators gives $l = 2$, leading to $F_{q,X} = 4(1-2p)^4 N^2 + 4\left[1 + 2(1-2p)^2 - 3(1-2p)^4\right] N$ and $F_{q,Z} = 4(1-2cp)^{2N} N^2$. In terms of scaling, this protocol is even worse than the bare GHZ protocol.

Remark 3. One might be concerned that although in all our protocols we have picked all the checks / stabilizers and all the phase imprinter to be local operators, the optimal measurement / symmetry operator is evidently non-local with a support spanning over the entire system. And, a measurement of such operator is generally not fault-tolerant. This is, indeed, used to be very concerning. However, recent development in fault-tolerant quantum computation has provided us a fault-tolerant way to measure such a non-local operator via local operators. This method is called "gauging logical operators" [28]. Similar to lattice surgery, the basic idea is, by introducing an ancilla system, we can turn a measurement of a non-local operator on our quantum code into a joint local measurement of operators involving

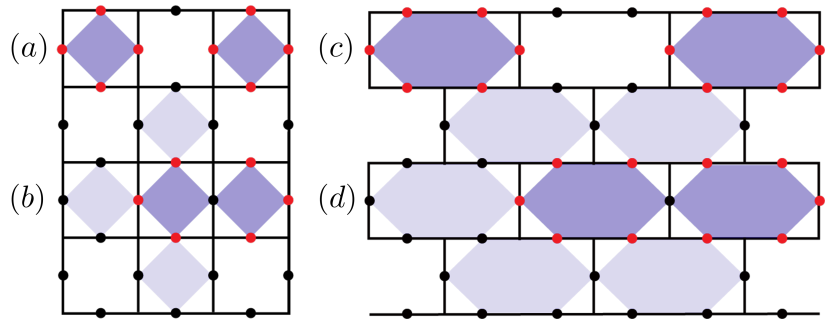

FIG. S1. F_X calculation for toric codes on square and honeycomb lattices. Square lattice: (a) one example of N^2 terms with prefactor $(1-2p)^8$; (b) one example of N terms with prefactor $4(1-2p)^6$. Honeycomb lattice: (c) one example of $O(N^2)$ terms with prefactor $(1-2p)^{12}$; (d) one example of N terms with prefactor $6(1-2p)^{10}$.

both the qubits of our quantum code and those of the ancilla system. We leave the modified partial error-correction protocol involving "gauging logical operators" to a future work.

Remark 4. We name a few more points that are beyond the scope of our work. Since our purpose is to introduce the partial QEC scheme, we have limited the analysis of our protocols in the simplest settings. First, we only considered errors on the physical qubits. A full error analysis that includes other types of circuit-level noise, such as noise from imperfect measurement, faulty gate implementation during syndrome extraction, or qubit loss (as seen, e.g. in Refs. [11, 44]) is left to future works. Second, we have not considered the most general decoherence model other than a mixture of X and Z noise before the phase imprinting and a general Pauli noise after the phase imprinting. Third, our discrete treatment of noise via quantum channels may miss features of the continuously applied signal and noise [45]. Apart from these, it would also be interesting to see how our current examples generalize to multi-parameter estimation tasks, where the commutation relations of the imprinters play a crucial role in determining the Fisher information matrix [46, 47].

QFI UNDER PERPENDICULAR NOISE

In this section, we provide a method to compute the QFI under perpendicular noise for different codes used in the main text. We first sketch the proof of a general statement: the QFI equals 4 times the variance of the generator of the imprinter (as in the pure state case), given the symmetry is strongly preserved. The proof can be also found in [11] and a closely related version in [31].

Consider a unitary phase imprinter $U(\theta) = e^{i\theta O}$ and a strong symmetry of the probe state $T_X\rho = t_x\rho$ that *anticommutes* with the generator O $\{T_X, O\} = 0$. Plugging into the error propagation formula, we have $\langle T_X\rangle_\theta = \mathrm{Tr}\left[\, U^\dagger(\theta)T_X U(\theta)\rho\right] = \mathrm{Tr}\left[\, U^{\dagger 2}(\theta)T_X\rho\right] = t_x \mathrm{Tr}\left[\, U^{\dagger 2}(\theta)\rho\right]$. Similarly, $\langle T_X^2\rangle_\theta = \mathrm{Tr}\left[\, U^\dagger(\theta)T_X^2 U(\theta)\rho\right] = \mathrm{Tr}\left[\, T_X^2\rho\right] = t_x^2$. Taylor expanding $U^\dagger(\theta)$, we obtain $\langle T_X\rangle_\theta = t_x\left[1 - 2\theta^2\langle O^2\rangle + \mathcal{O}(\theta^3)\right]$, yielding $\partial_\theta\langle T_X\rangle_\theta = t_x\left[-4\theta\langle O^2\rangle + \mathcal{O}(\theta^2)\right]$. Plugging back into the error propagation formula, we have:

$$\delta\theta^{-2} = \frac{\left|\partial_\theta\langle T_X\rangle_\theta\right|^2}{\langle T_X^2\rangle_\theta - \langle T_X\rangle_\theta^2} = \frac{t_x^2\left[-4\theta\langle O^2\rangle + \mathcal{O}(\theta^2)\right]^2}{t_x^2 - t_x^2\left[1 - 2\theta^2\langle O^2\rangle + \mathcal{O}(\theta^3)\right]^2} = 4\langle O^2\rangle + \mathcal{O}(\theta^3). \tag{S1}$$

Meanwhile, T_X also serves as the optimal measurement, in the sense that the QFI is *always* upper-bounded by the variance of O. Consequently, the propagated error saturates the CRB for $\theta \to 0$.

We finally remark that we do not assume T_X being hermitian or t_x being real. For a general unitary transform T_X, we refer interested readers to [11] for a construction of a POVM using Hadamard test, whose classical fisher information (CFI) saturates the QFI.

$F_{q,X}$ for GHZ state

We now compute the quantum Fisher information F_X for a GHZ with N qubits. From Eq. (S1), we know that it equals the variance of $O = \sum_j Z_j$. As this quantity remains linear in the density matrix ρ, it can be computed by

the dual channel trick

$$\langle O^2 \rangle_\rho = \langle E_X^\dagger [O^2] \rangle_{|\mathrm{GHZ}\rangle} \,. \tag{S2}$$

The action of the dual channel $E_X^\dagger$ on $O^2 = \sum_{i,j} Z_i Z_j$ can be counted by: (1) N^2 terms with prefactor $(1-2p)^2$, each coming from the identity $(1-p)Z_i + pX_iZ_iX_i = (1-2p)Z_i$; (2) subtraction of the N over-counted $i=j$ case that gives $Z_i^2 = 1$. Adding up two contributions, we have

$$F_{q,X} = 4(1-2p)^2 N^2 + 4\left[1-(1-2p)^2\right] N = 4(1-2p)^2 N^2 + 16\left[p(1-p)\right] N. \tag{S3}$$

$F_{q,X}$ for $|\mathrm{CSS}\rangle$ from toric codes

We move on to the $|\mathrm{CSS}\rangle$ constructed from toric codes on square and hexagonal lattices. We start with the square lattice where the imprinter is chosen as $O = \sum_p S_{Z,p}$, with each plaquette containing 4 physical qubits. As $\left\{\prod_{j\in -} X_j, O\right\} = 0$ and E_X strongly respects $\prod_{j\in -} X_j$, the $F_{q,X}$ can be calculated in the same way as $\langle O^2 \rangle = \sum_{p,p'} S_{Z,p} S_{Z,p'}$ using the dual-channel trick:

$$\langle O^2 \rangle_\rho = \langle E_X^\dagger [O^2] \rangle_{|\mathrm{CSS}\rangle} \,. \tag{S4}$$

Different from the GHZ state case, we now have three contributions in $\langle O^2 \rangle$: (1) N_Z^2 (number of S_Z stabilizers) terms with prefactor $(1-2p)^8$, coming from 8 physical qubits on two separated S_Z stabilizers (Fig. S1a); (2) subtraction of N_Z over-counted terms for $p = p'$ (here p is the label for the plaquette, not the error strength), which give $S_{Z,p}^2 = 1$; (3) subtraction of N_Z over-counted terms for adjacent $\langle p, p' \rangle$, which instead give a prefactor $4(1-2p)^6$ (Fig. S1b) for 6 physical qubits on 4 different directions. Adding up three contributions, we have

$$F_{q,X} = 4(1-2p)^8 N_Z^2 + 4\left[1 + 4(1-2p)^6 - 5(1-2p)^8\right] N_Z. \tag{S5}$$

For the toric code on the honeycomb lattice, a parallel geometric counting can be given as: (1) N_Z^2 terms with prefactor $(1-2p)^{12}$, coming from 12 physical qubits on separated $S_{Z,p}$ hexagons; (2) subtraction of N_Z over-counted terms for $p = p'$ and (3) subtraction of N_Z over-counted terms for adjacent $\langle p, p' \rangle$, which give a prefactor $6(1-2p)^{10}$ for 10 physical qubits on 6 different directions. Adding up three terms, we have

$$F_{q,X} = 4(1-2p)^{12} N_Z^2 + 4\left[1 + 6(1-2p)^{10} - 7(1-2p)^{12}\right] N_Z. \tag{S6}$$

QFI UNDER PARALLEL NOISE AND DECODING FOR PARTIAL ERROR CORRECTION

In this section, we provide analytical and numerical details in obtaining the $F_{q,Z}$ for various codes. We provide the details on how to conduct partial error correction for toric code construction.

Unlike the perpendicular noise, the parallel noise inevitably breaks the strong symmetry T_X. Specifically, for decoherence channel whose jump operator given by the phase imprinter, the no-go theorem states that the asymptotic scaling in N is at most linear [14, 19]. Nevertheless, we can still find possible advantages in polynomial suppression in the noise strength when the lattice size is finite, as this is also the case where a practical sensing task is conducted.

Let us begin with the GHZ state, then to the toric codes and Bacon-Shor codes.

$F_{q,Z}$ for GHZ state

Though it is well known that the GHZ state has an exponentially decaying QFI w.r.t. N. We find the derivation of it useful for later generalization. The GHZ state is a $+1$ eigenstate of the global $\mathbb{Z}_2$ symmetry $T_X = \prod_j X_j$. The i.i.d. Z (dephasing) channel breaks such strong symmetry: Consider a single site dephasing $E_{Z,i}[|\mathrm{GHZ}\rangle\langle\mathrm{GHZ}|] = (1-p)\,|\mathrm{GHZ}\rangle\langle\mathrm{GHZ}| + pZ_i\,|\mathrm{GHZ}\rangle\langle\mathrm{GHZ}|\,Z_i$, the dephased GHZ state has probability $P(+1) = 1-p$ of being in the $+1$ eigenspace of T_X and $P(-1) = p$ of being in the -1 eigenspace. The QFI $F_{q,Z}$ under such channel is then calculated as [15]

$$F_{q,Z} = 4\left[P(+) - P(-)\right]^2 N^2. \tag{S7}$$

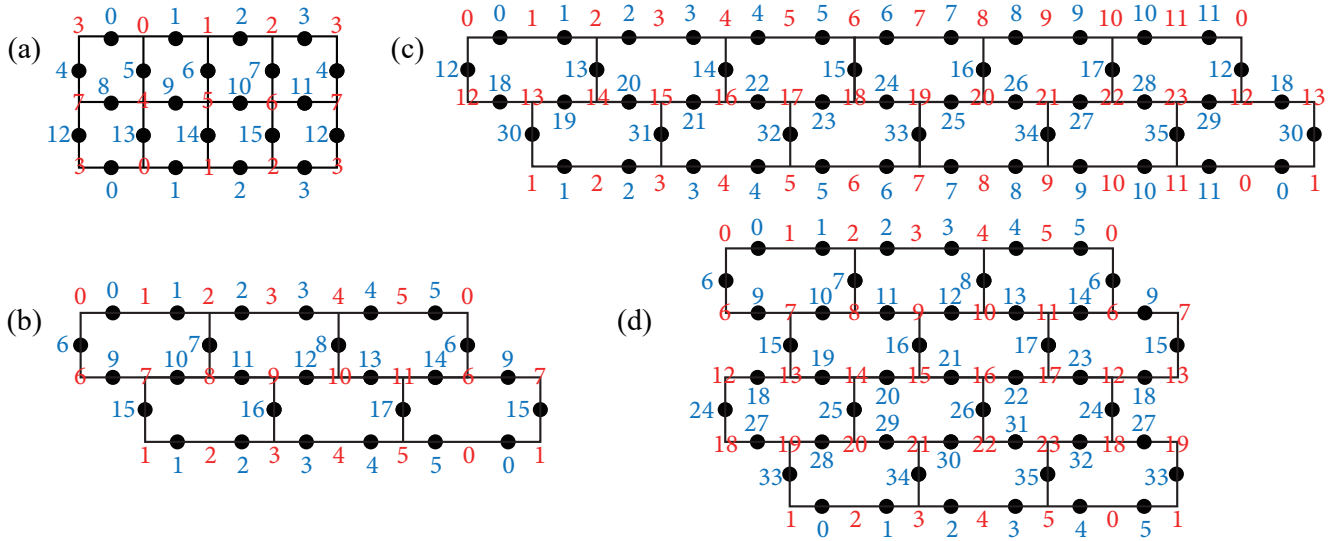

FIG. S2. Decoding examples for toric codes on square (a) and honeycomb (b)-(d) lattices with different lattice sizes and geometries. Different qubits are labeled by blue numbers and vertices by red numbers. For (c) and (d) we put the same amount of qubits on different lattice shapes.

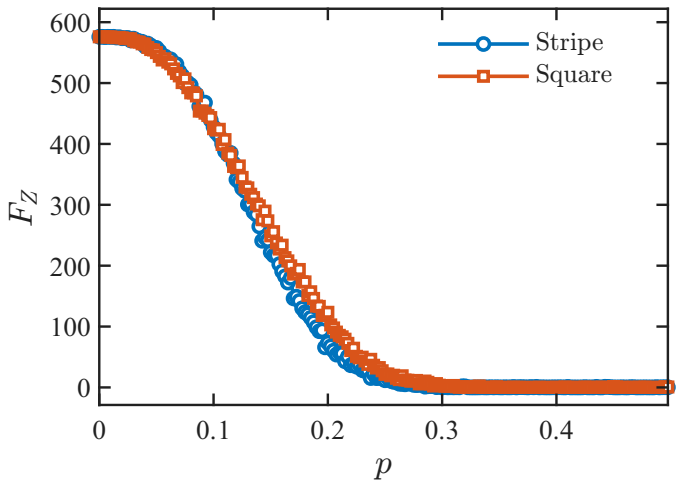

FIG. S3. Quantum Fisher information $F_{q,Z}$ as a function of the parameter p for two lattice configurations: stripe (Fig. S2c, circles, solid line) and square (Fig. S2d, squares, solid line). The data are obtained for a system of size $N = 36$. The plot shows that different choices of finite-size lattices does not significantly change the behavior of $F_{q,Z}$.

We note that this formula can be explicitly derived from the definition of the QFI $2\sum_{i,j}\frac{(\lambda_i-\lambda_j)^2}{\lambda_i+\lambda_j}\left|\langle\lambda_i|\sum_l Z_l|\lambda_j\rangle\right|^2$, as the only two candidates are $\frac{1}{\sqrt{2}}\left[|1\cdots 1\rangle \pm |-1\cdots -1\rangle\right]$ with probability $\lambda_+ = 1-p$, $\lambda_- = p$. For the i.i.d. Z noise, the only modification is $P(+) - P(-) = (1-2p)^N$. Substituting to Eq. (S7), we have

$$F_{q,Z} = 4(1-2p)^{2N}N^2. \tag{S8}$$

$F_{q,Z}$ for $|\mathrm{CSS}\rangle$ from toric codes

We now apply the above observation to the CSS probe state $|\mathrm{CSS}\rangle = \frac{1}{\sqrt{2}}\Big(|S_Z = 1\cdots 1\rangle + |S_Z = -1\cdots -1\rangle\Big)$. Consider the generalized dephasing channel

$$E_{S_Z}[\rho] = (1-p)\rho + pS_Z\rho S_Z, \tag{S9}$$

Vertices	Adjacency	Path
(0,1)	0,1,5,13/1,2,6,14	1
(0,2)	0,1,5,13/2,3,7,15	0,3
(0,3)	0,1,5,13/3,0,4,12	0
(0,4)	0,1,5,13/8,9,5,13	5
(0,5)	0,1,5,13/9,10,6,14	1,6
(0,6)	0,1,5,13/10,11,7,15	0,3,7
(0,7)	0,1,5,13/11,8,4,12	0,4
(1,2)	1,2,6,14/2,3,7,15	2
(1,3)	1,2,6,14/3,0,4,12	1,0
(1,4)	1,2,6,14/8,9,5,13	1,5
(1,5)	1,2,6,14/9,10,6,14	6
(1,6)	1,2,6,14/10,11,7,15	2,7
(1,7)	1,2,6,14/11,8,4,12	1,0,4
(2,3)	2,3,7,15/3,0,4,12	3
(2,4)	2,3,7,15/8,9,5,13	2,1,5
(2,5)	2,3,7,15/9,10,6,14	2,6
(2,6)	2,3,7,15/10,11,7,15	7
(2,7)	2,3,7,15/11,8,4,12	3,4
(3,4)	3,0,4,12/8,9,5,13	0,5
(3,5)	3,0,4,12/9,10,6,14	3,2,6
(3,6)	3,0,4,12/10,11,7,15	3,7
(3,7)	3,0,4,12/11,8,4,12	4
(4,5)	8,9,5,13/9,10,6,14	9
(4,6)	8,9,5,13/10,11,7,15	8,11
(4,7)	8,9,5,13/11,8,4,12	8
(5,6)	9,10,6,14/10,11,7,15	10
(5,7)	9,10,6,14/11,8,4,12	9,8
(6,7)	10,11,7,15/11,8,4,12	11

TABLE S1. Shortest paths between vertices for the 16-qubit toric code on the square lattice (Fig. S2a). The first column lists all possible pairs of vertices, whose adjacent qubits are given in the middle column. The shortest paths (sets of qubits) are given in the third column. The weight of one path is exactly the number of qubits it contains.

Vertices	Adjacency	Path	Vertices	Adjacency	Path
(0,1)	0,5,6/0,1,15	0	(3,8)	2,3,16/10,11,7	2,7
(0,2)	0,5,6/1,2,7	0,1	(3,9)	2,3,16/11,12,16	16
(0,3)	0,5,6/2,3,16	0,1,2	(3,10)	2,3,16/12,13,8	3,8
(0,4)	0,5,6/3,4,8	5,4	(3,11)	2,3,16/13,14,17	3,4,17
(0,5)	0,5,6/4,5,17	5	(4,5)	3,4,8/4,5,17	4
(0,6)	0,5,6/6,9,14	6	(4,6)	3,4,8/6,9,14	4,5,6
(0,7)	0,5,6/9,10,15	0,15	(4,7)	3,4,8/9,10,15	3,2,1,15
(0,8)	0,5,6/10,11,7	0,1,7	(4,8)	3,4,8/10,11,7	3,2,7
(0,9)	0,5,6/11,12,16	0,1,2,16	(4,9)	3,4,8/11,12,16	3,16
(0,10)	0,5,6/12,13,8	5,4,8	(4,10)	3,4,8/12,13,8	8
(0,11)	0,5,6/13,14,17	5,17	(4,11)	3,4,8/13,14,17	4,17
(1,2)	0,1,15/1,2,7	1	(5,6)	4,5,17/6,9,14	5,6
(1,3)	0,1,15/2,3,16	1,2	(5,7)	4,5,17/9,10,15	5,0,15
(1,4)	0,1,15/3,4,8	0,5,4	(5,8)	4,5,17/10,11,7	4,3,2,7
(1,5)	0,1,15/4,5,17	0,5	(5,9)	4,5,17/11,12,16	4,3,16
(1,6)	0,1,15/6,9,14	0,6	(5,10)	4,5,17/12,13,8	4,8
(1,7)	0,1,15/9,10,15	15	(5,11)	4,5,17/13,14,17	17
(1,8)	0,1,15/10,11,7	1,7	(6,7)	6,9,14/9,10,15	9
(1,9)	0,1,15/11,12,16	1,2,16	(6,8)	6,9,14/10,11,7	9,10
(1,10)	0,1,15/12,13,8	0,5,4,8	(6,9)	6,9,14/11,12,16	9,10,11
(1,11)	0,1,15/13,14,17	0,5,17	(6,10)	6,9,14/12,13,8	14,13
(2,3)	1,2,7/2,3,16	2	(6,11)	6,9,14/13,14,17	14
(2,4)	1,2,7/3,4,8	2,3	(7,8)	9,10,15/10,11,7	10
(2,5)	1,2,7/4,5,17	1,0,5	(7,9)	9,10,15/11,12,16	10,11
(2,6)	1,2,7/6,9,14	1,0,6	(7,10)	9,10,15/12,13,8	9,14,13
(2,7)	1,2,7/9,10,15	1,15	(7,11)	9,10,15/13,14,17	9,14
(2,8)	1,2,7/10,11,7	7	(8,9)	10,11,7/11,12,16	11
(2,9)	1,2,7/11,12,16	2,16	(8,10)	10,11,7/12,13,8	11,12
(2,10)	1,2,7/12,13,8	2,3,8	(8,11)	10,11,7/13,14,17	10,9,14
(2,11)	1,2,7/13,14,17	1,0,5,17	(9,10)	11,12,16/12,13,8	12
(3,4)	2,3,16/3,4,8	3	(9,11)	11,12,16/13,14,17	12,13
(3,5)	2,3,16/4,5,17	3,4	(10,11)	12,13,8/13,14,17	13
(3,6)	2,3,16/6,9,14	2,1,0,6			
(3,7)	2,3,16/9,10,15	2,1,15			

TABLE S2. Shortest paths between vertices for the 18-qubit toric code on the honeycomb lattice (Fig. S2b). The first column lists all possible pairs of vertices, whose adjacent qubits are given in the middle column. The shortest paths are given in the third column. The weight of one path is exactly the number of qubits it contains.

the resultant is again a mixture of $\frac{1}{\sqrt{2}}\Big(|S_Z = 1\cdots 1\rangle \pm |S_Z = -1\cdots -1\rangle\Big)$ with probability $P(+1) = 1-p$ and $P(-1) = p$. Further applying the i.i.d. S_Z noise, two probabilities satisfy $P(+1) - P(-1) = (1-2p)^{N_Z}$, with N_Z the number of S_Z stabilizers. Plugging into the defining equation of QFI, we obtain

$$F_{q,Z} = 4(1-2p)^{2N_Z} N_Z^2. \tag{S10}$$

Here, we assume that the dephasing channel being exactly the form in E_{S_Z}. If starting from the original i.i.d. Z noise, one should not directly apply the above formula. However, in the absence of logical error (even with logical error, one may still be able to derive the exact generalization of Eq. (S7), as there are only finitely many mixtures in the coding space), Eq. (S7) still applies as the state always remains a mixture of $\frac{1}{\sqrt{2}}\Big(|S_Z = 1\cdots 1\rangle \pm |S_Z = -1\cdots -1\rangle\Big)$ and the only modification is on $P(+) - P(-)$, which is determined by the error-correction and choice of decoding scheme. As stated in the main text, for a S_Z stabilizer with weight l, the least amount of Z error is $\frac{\lfloor l+1 \rfloor}{2}$, for which no decoding scheme is able to distinguish. We therefore expect that, when applying the i.i.d. Z noise and correction, $P(+) - P(-)$ is effectively described by $(1-p_{eff})^{2N_Z}$ with $p_{eff} = \alpha p^{\frac{\lfloor l+1 \rfloor}{2}}$. Compared with the exact S_Z dephasing channel, this formula is only approximate and we show by numerics to verify this approximation.

To see how the decoding and error correction are realized, we next provide several sample codes for different background lattices. We start with a simple 16-qubit toric code on the square lattice in Fig. S2a. We label qubits by blue numbers and vertices by red numbers. We also label the syndrome outcome by its vertex numbers. For example, when a Z error string connects 0 and 2, we have the syndrome outcome $S_{0,2} = -1$ while others 1. To apply the Minimum-Weight Perfect Matching (MWPM) decoder, we next assign minimum weights to all paths between vertices. As we are applying uniform errors to all physical qubits, the minimum weight is chosen as the shortest distance between two vertices. For the 16-qubit code, such shortest paths are given in Tab. S1, where the first column lists all possible pairs of vertices, the middle column lists the corresponding adjacent qubits for two vertices, and the third column computes the shortest path between them. The weight of a path is exactly the number of qubits it contains. For example, $(0,1)$ has weight 1 and $(0,6)$ has weight 3. After a round of syndrome measurement, we have even number of -1 syndromes. We then compute the minimum weight for all pairs of syndromes/vertices, and apply $Z's$ along the overall shortest paths. A parallel weight computation for the 18-qubit toric code on the honeycomb lattice (Fig. S2b) can be done with a different (shortest) path identification in Tab. S2.

To efficiently enlarge the lattice size $N \propto L_x \times L_y$ and to compute the QFI from classical syndrome patterns, we filter out the case where logical Z_L error happens. This is more likely for a "stripe"-like lattice (e.g. Fig. S2a,b,c)

around the shortest lateral size $min(L_x, L_y)$. However, we note that the probability of a logical error is much smaller than a stabilizer error. We therefore expect the QFI $F_{q,Z}$ to be determined by the bulk properties of the code and keep only patterns with no logical errors after error correction. For example, for the stripe lattice in Fig. S2a, we keep only patterns satisfying $X_4X_5X_6X_7 = 1$ and $X_0X_8 = 1$. Similarly, we require $X_6X_7X_8 = 1$ and $X_1X_{10} = 1$ for (b), $X_{12}X_{13}X_{14}X_{15}X_{16}X_{17} = 1$ and $X_1X_{19} = 1$ for (c), and $X_6X_7X_8 = 1$ and $X_1X_{10}X_{19}X_{28} = 1$ for (d). After this filtering, we expect the QFI F_Z is solely determined by the bulk property of the code rather than lattice shapes. Indeed, in Fig. S3, we observe only minor misalignment for stripe lattice in Fig. S2c and square lattice in Fig. S2d with identical number of qubits $N = 36$.

With this assumption, the QFI $F_{q,Z}$ can be explicitly computed using Eq. (S7), where $P(\pm) = \frac{n_\pm}{n_{tot}}$. $n_\pm$ here is, after error correction, the number of times that $X_0X_1X_2X_3 = \pm 1$ (enforced symmetry in the probe state) for Fig. S2a, $X_0X_1X_2X_3X_4X_5 = \pm 1$ for Fig. S2b, $X_0X_1X_2X_3 \cdots X_{11} = \pm 1$ for Fig. S2c, and $[X_0X_1X_2X_3X_4X_5]\,[X_{18}X_{19}X_{20}X_{21}X_{22}X_{23}] = \pm 1$ for Fig. S2d. Finally, $n = n_+ + n_-$ is the total repetitions of the numerics. This classical method can be directly applied to larger lattice sizes to compute the QFI F_Z, which is given in Fig.2 in the main text.

$F_{q,X}$ for $|\mathrm{CSS}\rangle$ from Bacon-Shor codes

The computation of $F_{q,X}$ (note the dephasing channel now contains i.i.d. X errors) is obtained by decoding via majority-voting, where an effective dephasing occurs only if half of the qubits in one row dephase, with the probability $p_{eff} = 1 - \sum_{k=0}^{\lfloor \frac{n-1}{2} \rfloor} \binom{n}{k} p^k (1-p)^{n-k}$. Eq. (S7) then yields

$$F_{q,X} = 4 \left[1 - 2 \sum_{k=0}^{\lfloor \frac{n-1}{2} \rfloor} \binom{n}{k} p^k (1-p)^{n-k} \right]^{2m} m^2. \tag{S11}$$

We also refer interested readers to [15] for further details.

QFI UNDER MIXTURE OF PARALLEL AND PERPENDICULAR NOISE FOR PARTIAL ERROR CORRECTION

In this appendix, we prove a major argument in the main text: The super-SQL scaling under both parallel and perpendicular noise persists to a mixture of them. To see this, we begin with a GHZ state under a mixture of i.i.d. Z and i.i.d. X noise, and then move on to the $|\mathrm{CSS}\rangle$ probe state.

We first explain what we mean by a mixture of i.i.d. Z and X noise. We focus on here when the error happens before the phase imprinting, postponing the discussion on error after the phase imprinting to the next appendix. In this setting, the more practical noise scenario is an application of i.i.d. Z ($\mathcal{E}_Z$) and i.i.d. X ($\mathcal{E}_X$) noise in an alternating manner, see Fig. S4a. Since two Pauli noise commute with each other: $\mathcal{E}_Z \cdot \mathcal{E}_X[\cdot] = \mathcal{E}_X \cdot \mathcal{E}_Z[\cdot]$, we can move all types of Z, X noise together, merging them into a single i.i.d. Z, X noise channel with larger strength p_Z, p_X. The commutation of Pauli channel allows us to first apply the Z noise (S4b) or X noise (S4c). Without loss of generality, we study the case where all i.i.d. X noise goes first.

Assume the total i.i.d. X noise takes the following form $\mathcal{E}_X = \prod_j \mathcal{E}_{X,j}$ with

$$\mathcal{E}_{X,j}[\rho] = (1 - p_X)\rho + p_X X_j \rho X_j, \tag{S12}$$

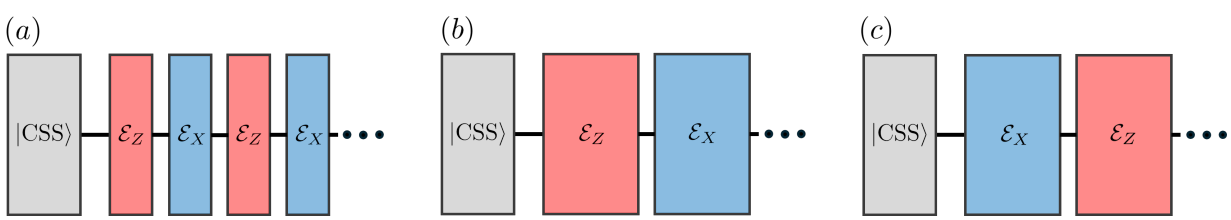

FIG. S4. A mixture of i.i.d. Z and X noise. The alternative application of Z and X in (a) is equivalent to first apply a total Z followed by a total X in (b) or first apply a total X followed by a total Z in (c).

the GHZ state after $\mathcal{E}_X$ becomes a mixture of $|s,\bar{s},+\rangle \equiv \frac{1}{\sqrt{2}}\left[|s\rangle + |\bar{s}\rangle\right]$, with $s = (s_1, s_2, ..., s_N) \in \{1,-1\}^N$ a binomial bit string recording the s_Z for each qubit. We introduce by $\bar{s}$ the binomial, bit-wise complement of s. Specifically, we have

$$\mathcal{E}_X\left[|\mathrm{GHZ}\rangle\langle\mathrm{GHZ}|\right] = \sum_{\{s,\bar{s}\}} p_{\{s,\bar{s}\}} |s,\bar{s},+\rangle\langle s,\bar{s},+| . \tag{S13}$$

Importantly, we have the orthogonality condition $\langle s_1,\bar{s}_1,+|s_2,\bar{s}_2,+\rangle = \delta_{s_1,s_2}$. The diagonal element $p_{\{s,\bar{s}\}} = p_X^{h(s)}(1-p_X)^{N-h(s)} + p_X^{N-h(s)}(1-p_X)^{h(s)}$ with $h(s) = \sum_j \frac{s_j+1}{2}$ the Hamming weight of the bit string that counts the number of spin $+1$. Plugging Eq. (S13) into the defining equation of the QFI, and note that $\sum_j Z_j |s,\bar{s},+\rangle = [N-2h(s)]|s,\bar{s},-\rangle$ with $|s,\bar{s},-\rangle \equiv \frac{1}{\sqrt{2}}\left[|s\rangle - |\bar{s}\rangle\right]$, we have

$$\begin{aligned}
F_{q,X} =& 2\sum_{\{s,\bar{s}\}} \frac{\left(p_{\{s,\bar{s}\}}-0\right)^2}{p_{\{s,\bar{s}\}}+0} \left|\langle s,\bar{s},+|\sum_j Z_j|s,\bar{s},-\rangle\right|^2 + 2\sum_{\{s,\bar{s}\}} \frac{\left(0-p_{\{s,\bar{s}\}}\right)^2}{0+p_{\{s,\bar{s}\}}} \left|\langle s,\bar{s},-|\sum_j Z_j|s,\bar{s},+\rangle\right|^2 && \text{(S14)}\\
=& 4\sum_{\{s,\bar{s}\}} p_{\{s,\bar{s}\}}\left[N-2h(s)\right]^2 && \text{(S15)}\\
=& 4\sum_{m=0}^{N}\binom{N}{m} p_X^m (1-p_X)^{N-m}(N-2m)^2 && \text{(S16)}\\
=& 4(1-2p_X)^2N^2 + 4\left[1-(1-2p_X)^2\right]N, && \text{(S17)}
\end{aligned}$$

where we have used the orthogonality $\langle s,\bar{s},+|s,\bar{s},-\rangle = 0$. We note that the last line is exactly 4 times the variance of $\sum_j Z_j$ with respect to $\mathcal{E}_X\left[|\mathrm{GHZ}\rangle\langle\mathrm{GHZ}|\right]$, which is derived conveniently from the symmetry argument in earlier context. Here, we write down another method to compute it, which is helpful when the variance argument breaks down for a broken strong symmetry.

We next apply the i.i.d. Z noise $\mathcal{E}_Z$ to the GHZ state. At this stage, no error correction is possible and a pure $|s,\bar{s},+\rangle$ becomes

$$\mathcal{E}_Z\left[|s,\bar{s},+\rangle\langle s,\bar{s},+|\right] = p_+ |s,\bar{s},+\rangle\langle s,\bar{s},+| + p_- |s,\bar{s},-\rangle\langle s,\bar{s},-| , \tag{S18}$$

with $p_\pm = \frac{1\pm(1-2p_Z)^N}{2}$ *independent* of $s,\bar{s}$. Therefore, the GHZ state after **both** $\mathcal{E}_X$ and $\mathcal{E}_Z$ can be diagonalized as

$$\mathcal{E}_Z\cdot\mathcal{E}_X\left[|\mathrm{GHZ}\rangle\langle\mathrm{GHZ}|\right] = \sum_{\{s,\bar{s}\}} p_{\{s,\bar{s}\}}\left(p_+ |s,\bar{s},+\rangle\langle s,\bar{s},+| + p_- |s,\bar{s},-\rangle\langle s,\bar{s},-|\right). \tag{S19}$$

Importantly, $|s,\bar{s},\pm\rangle$ form an orthogonal basis and, therefore, the QFI can be computed as

$$\begin{aligned}
F_{q,XZ} =& 2\sum_{s_1,s_2} \frac{\left(p_{\{s_1,\bar{s}_1\}}p_+ - p_{\{s_2,\bar{s}_2\}}p_-\right)^2}{p_{\{s_1,\bar{s}_1\}}p_+ + p_{\{s_2,\bar{s}_2\}}p_-} \left|\langle s_2,\bar{s}_2,+|\sum_j Z_j|s_1,\bar{s}_1,-\rangle\right|^2 && \text{(S20)}\\
&+ 2\sum_{s_1,s_2} \frac{\left(p_{\{s_1,\bar{s}_1\}}p_- - p_{\{s_2,\bar{s}_2\}}p_+\right)^2}{p_{\{s_1,\bar{s}_1\}}p_- + p_{\{s_2,\bar{s}_2\}}p_+} \left|\langle s_2,\bar{s}_2,-|\sum_j Z_j|s_1,\bar{s}_1,+\rangle\right|^2 && \text{(S21)}\\
=& 2\sum_{s_1,s_2} \frac{\left(p_{\{s_1,\bar{s}_1\}}p_+ - p_{\{s_2,\bar{s}_2\}}p_-\right)^2}{p_{\{s_1,\bar{s}_1\}}p_+ + p_{\{s_2,\bar{s}_2\}}p_-} \left[N-2h(s_1)\right]^2 \delta_{s_1,s_2} && \text{(S22)}\\
&+ 2\sum_{s_1,s_2} \frac{\left(p_{\{s_1,\bar{s}_1\}}p_- - p_{\{s_2,\bar{s}_2\}}p_+\right)^2}{p_{\{s_1,\bar{s}_1\}}p_- + p_{\{s_2,\bar{s}_2\}}p_+} \left[N-2h(s_1)\right]^2 \delta_{s_1,s_2} && \text{(S23)}\\
=& 4\left(p_+ - p_-\right)^2 \sum_s p_{\{s,\bar{s}\}}\left[N-2h(s)\right]^2 && \text{(S24)}\\
=& 4(1-2p_Z)^{2N}\left\{(1-2p_X)^2N^2 + \left[1-(1-2p_X)^2\right]N\right\} && \text{(S25)}\\
=& \frac{F_{q,X}F_{q,Z}}{4N^2}, && \text{(S26)}
\end{aligned}$$

where $F_{q,Z} = 4(1-2p_Z)^{2N}N^2$ is the QFI under *sole* $\mathcal{E}_Z$ noise and $F_{q,X}$ is the QFI under *sole* $\mathcal{E}_X$ noise given in Eq. (S17) for the GHZ state. We can easily see that the GHZ itself is fragile to a general mixture of X, Z noise even if its $F_{q,X}$ preserves the HL scaling, and the reason is a sub-SQL scaling in F_q, Z.

The same computation for $F_{q,XZ}$ can be done similarly as for the $|\text{CSS}\rangle$ state, by the following modification:

1. the bit string $s = (s_1, ..., s_{N_Z})$ now denotes the value of S_Z syndrome and the relevant $|s, \bar{s}, \pm\rangle$ are defined as

$$|s, \bar{s}, \pm\rangle = \frac{1}{\sqrt{2}} \left(|S_{Z,1} = s1, ...S_{Z,N_Z} = s_{N_Z}\rangle \pm |S_{Z,1} = \bar{s}1, ...S_{Z,N_Z} = \bar{s}_{N_Z}\rangle \right). \tag{S27}$$

Their orthogonality condition remains as $\langle s_1, \bar{s}_1, \pm|s_2, \bar{s}_2, \pm\rangle = \delta_{s_1,s_2}$ and $\langle s_1, \bar{s}_1, \mp|s_2, \bar{s}_2, \pm\rangle = 0$.

2. The expression for $p_{s,\bar{s}}$ is modified, whose $F_{q,X}$ is now directly computed as the variance of $\sum_j S_{Z,j}$, since the strong T_X symmetry is preserved. However, structurally, we still write $\mathcal{E}_X[|\text{CSS}\rangle\langle\text{CSS}|] = \sum_{s,\bar{s}} p_{\{s,\bar{s}\}} |s, \bar{s}, +\rangle\langle s, \bar{s}, +|$ and

$$F_{q,X} = 4 \sum_{\{s,\bar{s}\}} p_{\{s,\bar{s}\}} \left[N_Z - 2h(s)\right]^2 \tag{S28}$$

.

3. The expression for $p_\pm$ is also modified. Nevertheless, under the assumption that no logical Z error occurs, $p_\pm$ remains independent of $s, \bar{s}$ and $F_{q,Z}$ remains as Eq. (S7).

With the above clarification, we can write down $F_{q,XZ}$ in the exactly same structure as the GHZ state case, giving

$$\begin{aligned}
F_{q,XZ} =& 2 \sum_{s_1,s_2} \frac{\left(p_{\{s_1,\bar{s}_1\}}p_+ - p_{\{s_2,\bar{s}_2\}}p_-\right)^2}{p_{\{s_1,\bar{s}_1\}}p_+ + p_{\{s_2,\bar{s}_2\}}p_-} \left|\langle s_2, \bar{s}_2, +| \sum_j S_{Z,j} |s_1, \bar{s}_1, -\rangle\right|^2 && \text{(S29)}\\
&+ 2 \sum_{s_1,s_2} \frac{\left(p_{\{s_1,\bar{s}_1\}}p_- - p_{\{s_2,\bar{s}_2\}}p_+\right)^2}{p_{\{s_1,\bar{s}_1\}}p_- + p_{\{s_2,\bar{s}_2\}}p_+} \left|\langle s_2, \bar{s}_2, -| \sum_j S_{Z,j} |s_1, \bar{s}_1, +\rangle\right|^2 && \text{(S30)}\\
=& 2 \sum_{s_1,s_2} \frac{\left(p_{\{s_1,\bar{s}_1\}}p_+ - p_{\{s_2,\bar{s}_2\}}p_-\right)^2}{p_{\{s_1,\bar{s}_1\}}p_+ + p_{\{s_2,\bar{s}_2\}}p_-} \left[N_Z - 2h(s_1)\right]^2 \delta_{s_1,s_2} && \text{(S31)}\\
&+ 2 \sum_{s_1,s_2} \frac{\left(p_{\{s_1,\bar{s}_1\}}p_- - p_{\{s_2,\bar{s}_2\}}p_+\right)^2}{p_{\{s_1,\bar{s}_1\}}p_- + p_{\{s_2,\bar{s}_2\}}p_+} \left[N_Z - 2h(s_1)\right]^2 \delta_{s_1,s_2} && \text{(S32)}\\
=& 4\left(p_+ - p_-\right)^2 \sum_s p_{\{s,\bar{s}\}} \left[N_Z - 2h(s)\right]^2 && \text{(S33)}\\
=& \frac{F_{q,X}F_{q,Z}}{4N_Z^2}. && \text{(S34)}
\end{aligned}$$

An important difference is, as shown in the main text, by adaptively increasing the stabilizer weight $l(N)$ as a function of the number of physical qubits, we are able to keep both $F_{q,X}$ and $F_{q,Z}$ in the super-SQL region. Therefore, we expect that such a metrological advantage extends to the mixture case, where the QFI becomes a *multiplicative average*.

We note the denominator in Eq. (S34) is given by the number of stabilizers N_Z. Promoting to the ultimate bound given by the number of physical qubits N, we instead have:

$$F_{q,XZ} > \frac{F_{q,X}F_{q,Z}}{4N^2}. \tag{S35}$$

Suppose $F_{q,X} \sim N^{\nu_X}$ and $F_{q,Z} \sim N^{\nu_Z}$, then $F_{q,XZ}$ scales as $N^{\nu_X+\nu_Z-2}$, and therefore remains super-SQL for any mixture of X and Z noise for $\nu_X + \nu_Z > 3$. This is satisfied, for instance, in the Bacon-Shor code in Fig. 4a of the Letter, where $\nu_X + \nu_Z > 3.8$ at noise strength $p = 0.01$. When this condition fails, we are still safe as long as the noise strength is below a finite threshold. For example, rewrite $F_{q,X} = 4(1-p_X)^{2l}N_Z + O(N_Z)$, Eq. (S34) now becomes

$$F_{q,XZ} = (1-2p_X)^{2l}F_Z + O(N_Z^{-1}). \tag{S36}$$

In the Bacon-Shor codes, we observe that $l \sim O\left[\ln(N)\right]$ is sufficient to keep $F_{q,Z}$ a super-SQL scaling in N. In [15], it is further argued that this super-SQL scaling saturates the HL scaling $\nu_Z = 2$. Therefore, denoting $l = \alpha \ln N$, we can lower-bound $F_{q,XZ}$ via

$$F_{q,XZ} \geq (1-2p_X)^{2\alpha \ln N} F_{q,Z}. \tag{S37}$$

Therefore, as long as $p_X < \frac{1}{2}\left(1 - e^{\frac{1-\nu_Z}{2\alpha}}\right)$, we are safe for a super-SQL scaling in $F_{q,XZ}$.

PROOF TO THEOREM 1

Theorem 1. *The QFI of the probe state ρ_θ under i.i.d. Pauli errors described by $E_P[\rho_\theta] = (1 - p_x - p_y - p_z)\rho_\theta + p_x X\rho_\theta X + p_y Y\rho_\theta Y + p_z Z\rho_\theta Z$ + partial error correction is lower bounded by the QFI under the i.i.d. dephasing channel $\mathcal{E}_z[\rho_\theta] = (1-p)\rho_\theta + pZ\rho_\theta Z$+ partial error correction with the identification $p = p_y + p_z$.*

Proof. We choose the detection operator as T_X and evaluate $\langle T_X\rangle_\theta$ under E_P + error correction S_X. We first note that it has the same $\langle T_X\rangle_\theta$ as the i.i.d. channel $\mathcal{E}_j(\rho_\theta) = p_I\rho_\theta + p_x X_j\rho_\theta X_j + (p_y + p_z)Z_j\rho_\theta Z_j$+error correction, since $\{Z_j, T_X\} = \{Y_j, T_X\} = 0$ and the S_X stabilizers cannot distinguish them. As $[X_j, T_X] = 0$, it has identity action in $\langle T_X\rangle_\theta$ and therefore the same expectation value can be obtained by applying i.i.d. dephasing channel $\mathcal{E}_z[\rho_\theta] = (1 - p_z - p_y)\rho_\theta + (p_y + p_z)Z\rho_\theta Z$+error correction.

For $\mathcal{E}_z[\rho_\theta] = (1 - p_z - p_y)\rho_\theta + (p_y + p_z)Z\rho_\theta Z$+error correction, $\langle T_X\rangle_\theta = (1 - 2p_{odd})\cos(2N_Z\theta)$ with p_{odd} the probability that odd number of S_Z loop errors remain after correcting the S_X syndromes. The error propagation formula for $\langle T_X\rangle_\theta$ yields a lower bound for the QFI under the same channel as $F_q \geq 4(1 - 2p_{odd})^2 N_Z^2$, which exactly equals the QFI itself. Therefore, the QFI of ρ_θ under E_P + error correction S_X is lower bounded by the QFI under the i.i.d. dephasing channel $\mathcal{E}_z$+error correction S_X. □